CO_2 Laser Annealing for USJ Formation in Silicon: Comparison of Simulation and Experiment

Spyridon Stathopoulos, Antonios Florakis, Giorgos Tzortzis, Theodor Laspas, Andreas Triantafyllopoulos, Yohann Spiegel, Frank Torregrosa, and Dimitris Tsoukalas

***Abstract*— In this paper, we compare the experimental and simulation results of the effect of laser annealing on boron implanted silicon using a CO_2 source and commercially available process TCAD tools. The main objective of this analysis is the prediction of the evolution of temperature distribution induced into the wafer during the laser irradiation below the melting threshold as well as its effect on boron diffusion and activation kinetics. A series of factors are considered along with the use of advanced heat transfer and dopant diffusion models provided by the TCAD tool to accurately prototype the effect of the CO_2 irradiation on temperature and dopant distribution. These include the nonuniformity of the incident laser beam, the strong dependence of heat capacity and thermal conductivity from temperature and, most importantly, the dependency of the absorptivity from temperature and dopant distribution, which requires the solving of dopant and heat transfer equations in a coupled and self-consistent way. Using surface temperature data obtained by pyrometry measurements, it was possible to calibrate and to verify the validity of the results. Experimental boron profiles were then used to compare with simulations in the transient regime where dopant diffusion just starts to occur. Both TCAD and experimental data confirmed previous suggestions that submelt CO_2 laser annealing is an efficient tool for profile engineering, allowing diffusionless activation of the plasma doped boron profiles.**

***Index Terms*— Boron diffusion processes, CO_2 annealing, numerical simulation, silicon nonmelt annealing.**

I. Introduction

THE aggressive shrinking of the dimensions of modern field-effect transistor (FET) devices, as well as the development of newer FET implementations (such as FinFET), urge the use of novel annealing strategies for the formation of source/drain junctions, able to fulfill the demands imposed by the ITRS roadmap [1]. Among these, demonstration of high electrical activation levels and the minimization of boron diffusion is the driving force behind the implementation of ultra fast thermal processes such as spike, flash, and laser annealing.

Several different approaches regarding the wavelength (from UV to macro IR) and annealing duration (from femtosecond to millisecond) have been investigated. Among them, excimer [2] and all solid state lasers [3], in the nanosecond and millisecond time scale, respectively, are the most promising candidates. On the other hand, p-polarized carbon dioxide lasers have been recently embedded in commercial wafer irradiation systems, as they exhibit manufacturing–related advantages comparing with other laser sources of lower wavelength. CO_2 operation ($\lambda = 10.6\ \mu$m) at Brewster's angle reduces significantly reflectivity associated pattern dependency [4], a critical issue in the CMOS fabrication flow.

The complexity of the interaction between the silicon and CO_2 laser radiation stems from the very nature of absorption mechanisms, attributed mainly to photoexcitation of thermally active free carriers. Energy is transferred from excited carriers to lattice via electron-phonon scattering (in the time range 10^{-12}–10^{-13} s) resulting to local heating of lattice and an exponential rise of the absorption coefficient. Simultaneously, absorption length reduces significantly, forcing the optical absorption to take place in a smaller volume. Additionally, temperature rise is further enhanced by a decrease in thermal conductivity. All these factors combined, may lead to a dramatic increase of the overall heating rate, especially for irradiations in the nanosecond range, as the whole process is highly adiabatic [5], [6]. In the millisecond regime, which is the subject of this paper, the effect of the optical confinement is less prominent, as the longer annealing duration facilitates higher thermal dissipation within the silicon bulk.

In [7], we have investigated the implementation of carbon dioxide laser annealing for the formation of p-type ultra shallow junctions, conducting a multiparameter analysis. Based on our results [7], a new set of experiments has been performed, strictly in the submelt region, to compare the experimental results with TCAD simulations. The experiments include plasma doping, laser annealing, secondary ion mass spectrometry (SIMS) characterization and sheet resistance measurements of the samples. Various annealing conditions used represent a transient regime, where we are gradually

Manuscript received April 12, 2013; revised October 4, 2013, November 14, 2013, and December 21, 2013; accepted December 30, 2013. Date of publication January 24, 2014; date of current version February 20, 2014. This work was supported in part by the European Union and in part by the Greek National Funds through the Operational Program "Education and Lifelong Learning" of the National Strategic Reference Framework-Research Funding Program: "Heracleitus II. Investing in knowledge society through the European Social Fund." The review of this paper was arranged by Editor S. Deleonibus.

S. Stathopoulos, G. Tzortzis, T. Laspas, A. Triantafyllopoulos, and D. Tsoukalas are with the Department of Physics, School of Applied Sciences, National Technical University of Athens, Athens 15780, Greece (e-mail: spystath@mail.ntua.gr; geotzort@mail.ntua.gr; the.laspas@gmail.com; triandreas@hotmail.com; dtsouk@central.ntua.gr).

A. Florakis was with the National Technical University of Athens, School of Applied Sciences, Athens 15780, Greece. He is now with IMEC, Leuven 3001, Belgium (e-mail: florakis@imec.be).

Y. Spiegel and F. Torregrosa are with Ion Beam Services, Peynier 13790, France (e-mail: yohann.spiegel@ion-beam-services.fr; frank.torregrosa@ion-beam-services.fr).

Color versions of one or more of the figures in this paper are available online at http://ieeexplore.ieee.org.

Digital Object Identifier 10.1109/TED.2014.2299311

0018-9383 © 2014 IEEE. Personal use is permitted, but republication/redistribution requires IEEE permission.
See http://www.ieee.org/publications_standards/publications/rights/index.html for more information.

crossing the barrier from a diffusionless to a net dopant movement process.

Additionally, we have developed a TCAD procedure for the simultaneous description of the effect of laser annealing on the temperature distribution evolution coupled with boron diffusion kinetics using the Synopsys Sentaurus process TCAD tool (SProcess) [8]. Simulation with SProcess pertains to all aspects of the process from dopant implantation to annealing and diffusion.

II. Experiment

Boron ions have been introduced into n-type silicon wafers using low energy BF_3 plasma immersion ion implantation (PIII) technique using the PULSION tool developed by IBS [9]. The nominal values of acceleration voltage (i.e., the energy of the implantation) and dose were 0.6 kV and 1×10^{15} cm^{-2}, respectively. The actual dose of the implantation was found out to be around 55% of the nominal value. To annihilate the damage induced by the implantation and improve the electrical characteristics of the junction, the samples are thermally treated using a CO_2 laser. Details for the CO_2 laser irradiation setup, which has been used are given elsewhere [7]. Using a fixed laser power value of 64 W, we have performed several irradiations modifying the spot diameter and the pulse duration to determine the optimum annealing conditions. At the final set of irradiations, laser beam has been focused to a spot of 1.1 mm in diameter at around 9400 W$\cdot$cm^{-2} peak power density and the pulse duration was in the range 6–10 ms (56–94-J$\cdot$cm^{-2} energy density, respectively). However, to conduct more reliable temperature measurements using the infrared pyrometer, several experiments were conducted using larger spots and longer pulses. The results obtained from real time pyrometry were used for the validation of the calculations regarding the laser—silicon thermal interaction and the peak temperature values determined by this process were used for the evaluation of the thermal predictions. In all the experiments, samples are mounted vertically upon a heating base. Wafer preheating is necessary to increase the light absorption rate at the beginning of the irradiation process. As absorption coefficient has an exponential dependence on temperature, preheating can lead to significantly higher peak temperatures for the same duration and power fluency values. Peak surface temperature ranges from 1250 °C to 1400 °C, depending on the duration of the laser pulse. SIMS analysis was carried out with a Cameca IMS 4fE6 instrument. Preliminary SIMS measurements showed that the preheating of the samples for 1 to 2 min at 650 °C does not modify the dopant profile. Considering the restrictions imposed by the SIMS detection limit no parasitic diffusion has been observed.

As the intensity distribution of the beam is Gaussian, the annealing effect (and consequently the postannealing doping profile) is inherently not uniform. Hence, the mapping of sheet resistance distribution is necessary and several sheet resistance measurements have been performed across the irradiated area. As the deviation in the sheet resistance measurements values, obtained in the central region of the beam, is small it is possible to get a reliable averaged value. Sheet resistance measurements were performed using the van der Pauw four point probe technique on a prober equipped with an optical microscope. The probes were arranged in square geometry and their distance was about 100 μm. Additionally, by performing a deep circular cut using a diamond pen around the perimeter of the irradiated area before the characterization, we have ensured the lateral electrical isolation of the region. In addition, gold contacts have been fabricated using e-gun evaporation to minimize the contact resistance. Based on sheet resistance cartography of the laser annealed area, SIMS measurements were conducted, aiming in the central beam area that we have measured a minimum sheet resistance, so as to monitor the maximum possible diffusion of the dopant profile.

III. Simulation and Discussion

A. Thermal Distribution

Two-dimensional effects have to be considered for the CO_2 simulation. In addition, the absorption coefficient must be calculated at each time step and for each node of the simulation mesh, as it is strongly dependent on dopant distribution and temperature. To describe the absorption coefficient, we followed the approximation introduced by [10] given in (1)

$$\alpha(N,T) = 1.9 \times 10^{-20} T^{3/2} \times \left[N + 3.87 \times 10^{16} \left(\frac{T}{300}\right)^{3/2} \exp - \frac{7020}{T}\right] + 2 \tag{1}$$

where N represents the free carrier concentration and T the temperature at each node. This strong coupling between the absorption coefficient and both temperature and boron distributions may give rise to transient phenomena, such as thermal lensing, which will lead eventually in steep temperature increase, especially for very short pulses (nanosecond or less). In the millisecond regime, however, there is enough time for efficient heat dissipation toward the bulk, as it is depicted from the thermal length l_{thermal} dependency on the square root of pulse duration. Overall, as it will be shown later, the relatively long annealing times, lead to a wider thermal distribution and thus reduce eventually the temperature rise.

Regarding the programmatic description of the laser intensity distribution profile, Sentaurus Process assumes that the incident beam is spatially uniform and has a Gaussian-like time evolution. This approach is typical for pulsed lasers (such as excimer or solid state) but is insufficient for the simulation of the CO_2 laser, which is constant wave. Therefore, the intensity profile must be incorporated manually through a user-defined function, which is constant with time and has a Gaussian spatial distribution to reflect the 00 transverse electromagnetic mode (TEM_{00}) of the laser. Then, only the beam diameter, lateral dimensions of the calculation field and the incident power density are required to accurately reproduce the intensity profile as far as the simulator is concerned. It should be apparent that the description of the profile is strictly 2-D. A series of 1-D calculations has also been performed, mainly for calibration reasons, but it was unable to reproduce any experimental data and it was depreciated in favor of the 2-D approach.

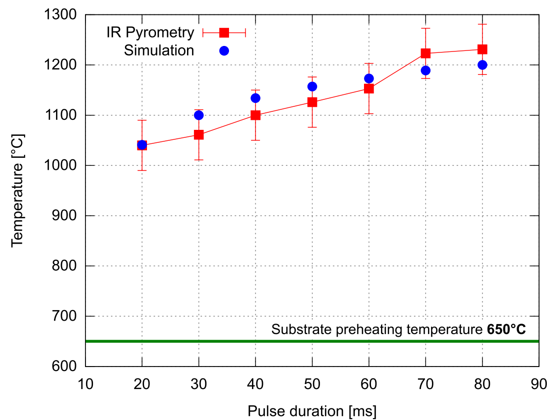

Fig. 1. Peak surface temperature for several laser pulse duration values, obtained by simulation (blue dots) and IR pyrometry (red squares). Excellent level of agreement has been achieved for almost every annealing condition. Laser was focused on a spot size diameter of 1.8 mm, at a sample sustained at 650 °C.

The temperature dependence of every parameter included in heat equation [11] was considered. Since the characteristic lengths of dopant and thermal diffusion effects differ more than one order of magnitude, mesh structure was properly modified so that both physical phenomena could accurately be simulated. This necessitates the use of a dense mesh (less than 1 nm) near the surface area, where dopant diffusion is studied, letting it become coarser toward silicon wafer bottom (extending down to 700-μm depth). On the other hand, as absorption coefficient depends on dopant concentration, a possible profile movement should be considered, as diffusion leads to lower concentration profiles and thus lower absorption values. As it will be discussed in the next section, the advanced models set of models has been used during simulations.

Even though the most promising irradiation results have been obtained by focusing the laser beam at a spot size of 1.1 mm and pulse duration of 6–10 ms for calibration and verification reasons, we started our analysis with larger spots and longer annealing times due to limitation imposed by the IR pyrometer spot size (0.6 mm) and sampling rate (500 Hz) to increase the reliability of the process. This way, we have validated our simulation results with peak temperature values, which have been reached after several tens of milliseconds. The results of this experiment are shown in Fig. 1, which presents a comparison for the peak surface temperatures obtained by simulation and IR pyrometry. Excellent agreement has been achieved for every pulse duration supporting the validity of our calculations while being consistent with [12].

Subsequently, we have investigated a time range that is relevant for USJ technology for which the laser had to be focused in a smaller area (leading to higher temperature rise rate). The minimization of annealing time is critical, to reduce boron diffusion. Many parameters affect the temperature evolution including pulse duration, preheating temperature and doping concentration. The last two factors affect the process indirectly by modifying the absorption coefficient of silicon. Different combinations have been considered, however, only the most promising results are presented in this paper. Three different pulse durations (6, 8, and 10 ms) have been used while keeping the other parameters constant (1×10^{15} cm^{-2} at 0.6 kV for the doping and 650 °C for the preheating temperature).

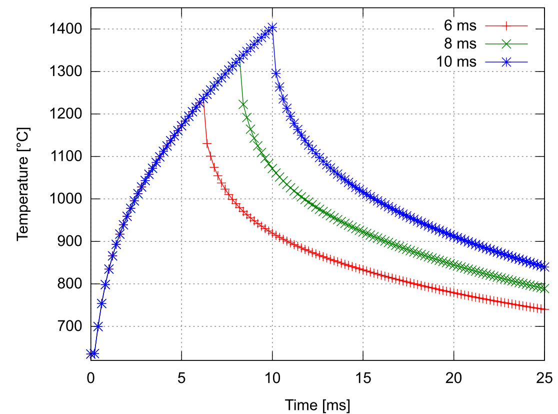

Fig. 2. Calculated average surface temperature for three different pulse durations. Irradiations performed at a spot size diameter of 1.1 mm, while the preheating temperature was 650 °C. All cases are below the melting point of silicon (1410 °C).

Fig. 2 shows the calculated evolution of surface temperature with time for three different pulse durations, for a sample preheated at 650 °C. As it can be observed by the simulation, no melting occurred in any of the cases. However, the 10 ms case being very close to the melting point of silicon, gave rise to more prevalent diffusion, as it can be observed by the SIMS measurements discussed later.

Fig. 3 shows the 2-D snapshots of temperature distribution within silicon bulk, for two different values of pulse duration (6 and 10 ms). The shape of the isothermal lines reflects the Gaussian spatial distribution of the beam intensity. These snapshots were captured at the end of the pulse (where the overall temperature distributions reach their maximum value). Results for the rest of the irradiation combinations are similar. The temperature distribution within silicon bulk at the corresponding conditions is shown in Fig. 4. All curves have been extracted at the time where the maximum surface temperature was reached for each annealing condition.

B. Simulation of Boron Diffusion and Activation Kinetics

Following the thermal analysis, we proceeded to investigate the diffusion and activation of the boron dopants. Starting with the doping step we have used the plasma doping routines of SProcess (version 2012.09). Since SProcess does not readily support the PIII process we have broken down the implantation process to several BF_2 steps. The dose and energy of these steps have been selected so that the resultant boron distribution resembles the SIMS as-implanted data as closely as possible. More elaborate modeling of PIII is possible [13] but it is beyond the scope of this paper. The rest of the simulation was carried out with the version 2009.06 of the tool.

SProcess solves simultaneously the heat equation along with the relevant transport and clustering equations related to dopants for each node. This fact, allows for a self-consistent description of the coupling of the thermal and diffusion related transient phenomena that take place during the annealing. For an accurate modeling of the dopant diffusion and activation kinetics, we have implemented the advanced models set of

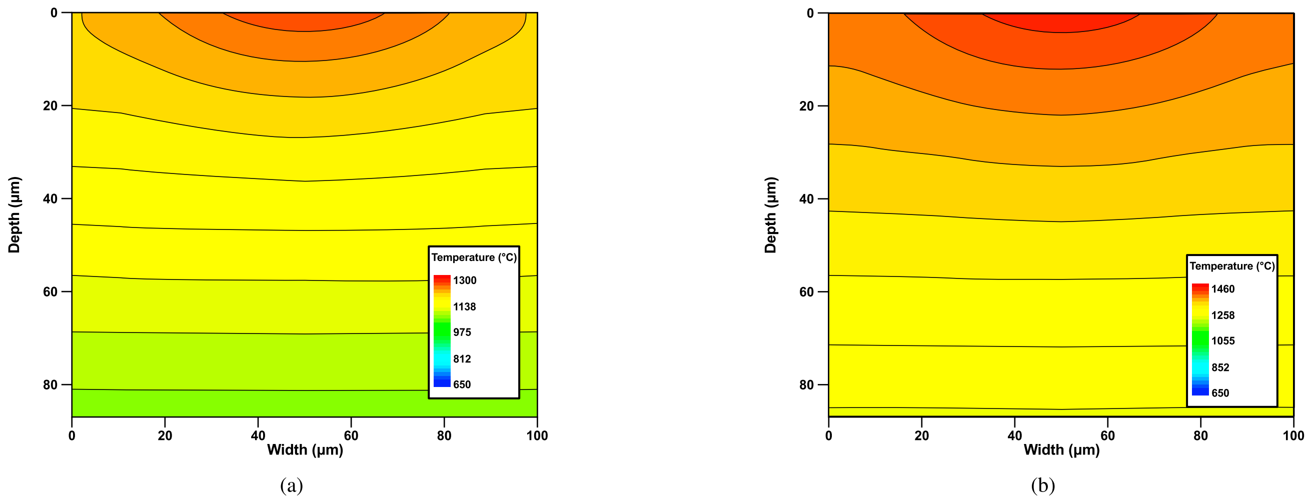

Fig. 3. Isothermal lines indicating temperature distribution within silicon bulk. Each snapshot has been obtained at the end of the pulse (where the maximum surface temperature was reached), for two different pulse durations; 6 and 10 ms. (a) Snapshot at 6 ms. (b) Snapshot at 10 ms.

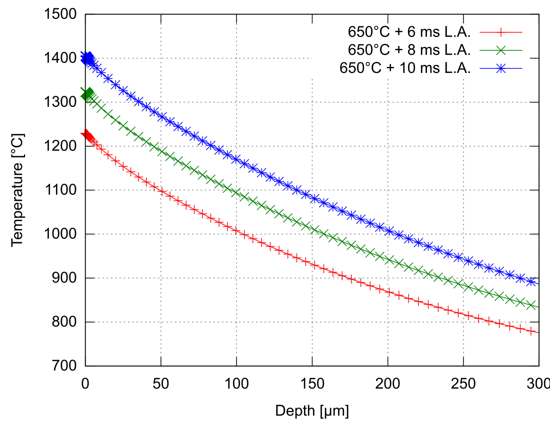

Fig. 4. Simulated average temperature distribution for the three different pulse durations. Each snapshot was taken at the end of the corresponding pulse.

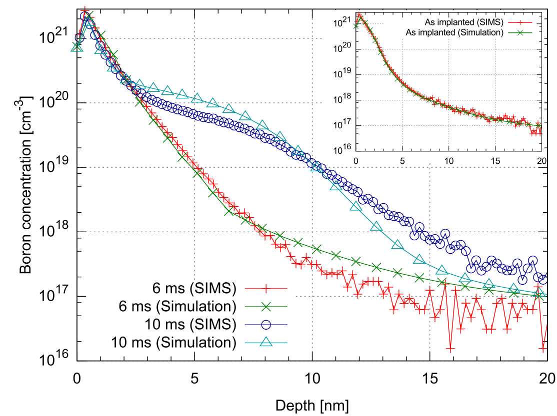

Fig. 5. Comparison of the boron distribution as calculated by Sentaurus process and actual SIMS data. In the case of 10 ms significant, diffusion can be observed whereas in the case of 6 ms there is no apparent movement of the profile distribution. In the inset simulated and actual boron as implanted profile.

models [14]. The main features of this combination of models and updated parameters are the charged-react model for the dopant transport, the charged-cluster for the boron clustering with interstitials and the full model for the interstitial clustering evolution.

Charged-react is a five-stream model, considering an immobile substitutional dopant and up to two mobile charged dopant—defect pair species. Mobile charged point defects are also included. For the solution of the system of equations, a variety of phenomena related with dopant and point defects kinetics are considered [15], [16]. Moreover, the effect of the presence of the co-implanted fluorine molecules has been included. The implementation of charged-cluster allows for the description of boron interstitial clusters (BICs), which are a prominent damage configuration and can affect the boron kinetics and activation levels. The full model can monitor the complete evolutionary path of interstitials—consisted defects, from small interstitial clusters to {311} defects as well as dislocation loops.

Fig. 5 compares the actual dopant distribution for two different laser annealing conditions (6 and 10 ms) with the corresponding simulation results. The initial profile used in the simulations is shown in the inset of Fig. 5 and it is in excellent agreement with the SIMS data. As we can observe for the annealed samples, the case of 6 ms exhibits minimal diffusion whereas in the case of 10 ms, the diffusion is more prominent since surface temperature reached quite close to the melting point of silicon (1410 °C). In both cases, the agreement between the simulated and experimental results is very good.

We can also observe that experiments and simulations capture the immobile boron profile contained at the top 3 nm with the threshold concentration of mobile boron close to 2×10^{20} cm^{-2} as previously observed [15]. This immobile part of boron profile at high concentrations has been attributed to the formation of various sizes BICs observed by [15] through TEM imaging and successfully initially simulated by [17].

Moreover, the simulation of boron diffusion kinetics allowed us to determine the distribution of the activated boron atoms. In conjunction with the total diffused boron distribution, the sheet resistance of the sample in the irradiated area can be calculated. In Fig. 6, the evolution of the sheet resistance

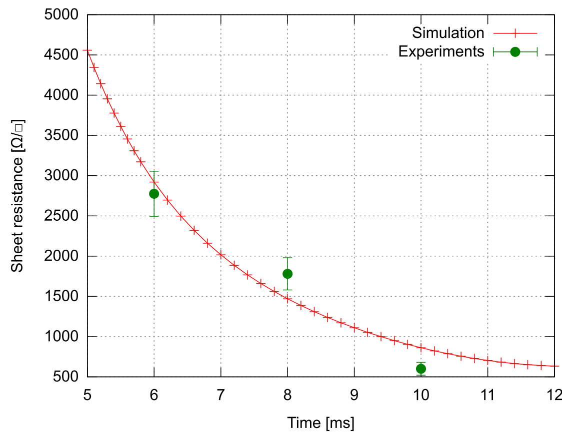

Fig. 6. Evolution of the sheet resistance for three samples irradiated with three CO_2 pulses of different durations as compared with the sheet resistance calculated for the activated boron profile extracted from the simulations. The experimental data are the averaged values of the area sustained the top of the Gaussian beam.

in the annealed area is depicted along with the experimental values determined by averaging the van der Pauw measurements in the central region of the irradiation, which was subjected to the highest laser intensity. To build the simulated curve of Fig. 6, the total (N) and active (N_B) boron profiles have been extracted in every time step of the simulation. Then, the integral $\int N_B(x)\mu(N(x),x)dx$, has been calculated for each step to extract the simulated sheet resistance values (μ being the mobility of carriers). The case of 10 ms displays slightly lower sheet resistance than the calculated value; however, this is to be expected because 10 ms is a fringe case as it has been already discussed. It is apparent, however, that the CO_2 irradiation significantly improves the electrical behavior of the junction even though the induced dose used is very low. The results of the 10 ms case are similar or better to others obtained by nonmelt annealing procedures [18]–[20]. A higher implantation dose should further reduce the resistance toward the figure of merit.

IV. Conclusion

This paper is part of a wider investigation of the implementation of submelt CO_2 laser annealing for ultra shallow junction formation. Due to the reduced pattern dependence, long wavelength irradiation is especially suitable for nonplanar architectures, such as FinFET devices, for example. Using process TCAD, we were able to describe the interaction of laser and silicon, both in terms of temperature evolution, dopant diffusion and activation kinetics. At high wavelengths carrier photogeneration is the dominant mechanism for absorption, so the latter is strongly coupled with the carrier concentration and temperature. The adequate level of agreement between the simulation results and IR pyrometry measurements, indicates the effectiveness of the modeling approach. Experimental and simulation results revealed a significant reduction of sheet resistance, while the movement of boron concentration profile was minimal. Irradiations at higher intensities and shorter durations can further improve these results, constituting nonmelt CO_2 laser annealing a promising alternative to conventional spike thermal treatment.

Acknowledgment

The authors would like to thank Dr. G. Bennassayag (CEMES/CNRS) for conducting the SIMS measurements of the samples used for the experiments. The authors also heartily thank Prof. C. Grigoropoulos (Laser Thermal Lab, University of California, Berkeley) for helpful discussions regarding thermal modeling.

References

[1] (2012). *International Technology Roadmap for Semiconductors* [Online]. Available: http://www.itrs.net/Links/2012ITRS/2012Chapters/2012Overview.pdf
[2] K. K. Ong, K. L. Pey, P. S. Lee, A. T. S. Wee, X. C. Wang, and Y. F. Chong, "Dopant activation in subamorphized silicon upon laser annealing," *Appl. Phys. Lett.*, vol. 89, no. 8, pp. 082101-1–082101-3, 2006.
[3] B. Mizuno and Y. Sasaki, "Aiming for the best matching between ultra-shallow doping and milli-to femto-second activation," in *Proc. 15th Int. Conf. Adv. Thermal Process. Semicond.*, Oct. 2007, pp. 1–10.
[4] L. Feng, Y. Wang, and D. Markle, "Minimizing pattern dependency in millisecond annealing," in *Proc. Int. Workshop J. Technol.*, 2006, pp. 25–30.
[5] D. Bäuerle, *Laser Processing and Chemistry*. New York, NY, USA: Springer-Verlag, 2011.
[6] J. Narayan, R. B. James, O. W. Holland, and M. J. Aziz, "Pulsed excimer and CO_2 laser annealing of ion-implanted silicon," *J. Vac. Sci. Technol.*, vol. 3, no. 4, pp. 1836–1838, Jul. 1985.
[7] A. Florakis, E. Verrelli, D. Giubertoni, G. Tzortzis, and D. Tsoukalas, "Non-melting annealing of silicon by CO_2 laser," *Thin Solid Films*, vol. 518, no. 9, pp. 2551–2554, Feb. 2010.
[8] *Sentaurus Process User Guide*, Synopsys Inc., Mountain View, CA, USA, 2012.
[9] S. B. Felch, F. Torregrosa, H. Etienne, Y. Spiegel, L. Roux, and D. Turnbaugh, "Pulsion HP: Tunable, high productivity plasma doping," *AIP Conf. Proc.*, vol. 1321, no. 1, pp. 333–336, Jan. 2011.
[10] M. Blomberg, K. Naukkarinen, T. Tuomi, V.-M. Airaksinen, M. Luomajarvi, and E. Rauhala, "Substrate heating effects in CO_2 laser annealing of ion-implanted silicon," *J. Appl. Phys.*, vol. 54, no. 5, pp. 2327–2328, 1983.
[11] W. Szyszko, "Melting and diffusion under nanosecond laser pulse," *Appl. Surf. Sci.*, vol. 90, no. 3, pp. 325–331, Nov. 1995.
[12] M. Doubenskaia, P. Bertrand, and I. Smurov, "Pyrometry in laser surface treatment," *Surf. Coat. Technol.*, vol. 201, no. 5, pp. 1955–1961, 2006.
[13] Z. Essa, F. Cristiano, Y. Spiegel, P. Boulenc, Y. Qiu, M. Quillec, *et al.*, "BF_3 PIII modeling: Implantation, amorphisation and diffusion," *AIP Conf. Proc.*, vol. 1496, no. 1, pp. 237–240, 2012.
[14] *Sentaurus Advanced Calibration for Process Simulation Guide*, Synopsys Inc., Mountain View, CA, USA, 2012.
[15] F. Cristiano, X. Hebras, N. Cherkashin, A. Claverie, W. Lerch, and S. Paul, "Clusters formation in ultralow-energy high-dose boron-implanted silicon," *Appl. Phys. Lett.*, vol. 83, no. 26, pp. 5407–5409, Dec. 2003.
[16] E. Lampin, F. Cristiano, Y. Lamrani, A. Claverie, B. Colombeau, and N. E. B. Cowern, "Prediction of boron transient enhanced diffusion through the atom-by-atom modeling of extended defects," *J. Appl. Phys.*, vol. 94, no. 12, pp. 7520–7525, 2003.
[17] M. Aboy, L. Pelaz, E. Bruno, S. Mirabella, and S. Boninelli, "Kinetics of large B clusters in crystalline and preamorphized silicon," *J. Appl. Phys.*, vol. 110, no. 7, pp. 073524-1–073524-14, 2011.
[18] S. R. Aid, S. Matsumoto, G. Fuse, and S. Sakuragi, "Comparison of boron diffusion in silicon during shallow p^+/n junction formation by non-melt excimer and green laser annealing," *Phys. Status Solidi (A)*, vol. 208, no. 12, pp. 2772–2777, 2011.
[19] A. Florakis, A. Papadimitriou, N. Chatzipanagiotis, N. Misra, C. Grigoropoulos, and D. Tsoukalas, "Formation of silicon ultra shallow junction by non-melt excimer laser treatment," *Solid-State Electron.*, vol. 54, no. 9, pp. 903–908, Sep. 2010.
[20] J. Sharp, N. Cowern, R. Webb, K. Kirkby, D. Giubertoni, S. Gennaro, *et al.*, "Deactivation of ultrashallow boron implants in preamorphized silicon after nonmelt laser annealing with multiple scans," *Appl. Phys. Lett.*, vol. 89, no. 19, pp. 192105-1–192105-3, 2006.

Spyridon Stathopoulos received the Diploma degree in applied physics in 2009 and the M.Sc. degree in microelectronics and nanotechnology in 2011 from the School of Applied Sciences, National Technical University of Athens (NTUA), Athens, Greece, where he is currently pursuing the Ph.D. degree.

Antonios Florakis received the Diploma degree in applied physics and the M.Sc. degree in microelectronics and nanotechnology from the National Technical University of Athens (NTUA), Athens, Greece, in 2005 and 2006, respectively, and the Ph.D. degree from the School of Applied Sciences, NTUA, in 2011.

He has been with IMEC, Leuven, Belgium, since 2011, as a Post-Doctoral Fellow.

Giorgos Tzortzis received the Diploma degree in mechanical engineering from the School of Mechanical Engineering, National Technical University of Athens (NTUA), Athens, Greece, in 2007, and the M.Sc. degree in microelectronics and nanontechnology from the School of Naval Engineering, NTUA, in 2009, where he is currently pursuing the Ph.D. degree.

He has been with the School of Naval Engineering, NTUA, since 2010.

Theodor Laspas received the Diploma degree in applied physics from the School of Applied Sciences, National Technical University of Athens, Athens, Greece, in 2010. He is currently pursuing the M.Sc. degree in production engineering with the School of Industrial Engineering and Management, Royal Institute of Technology, Stockholm, Sweden.

His current research interests include machine tool metrology, machining system dynamics, and manufacturing technology.

Andreas Triantafyllopoulos received the Diploma degree from the School of Applied Sciences, National Technical University of Athens, Athens, Greece, in 2012.

Yohann Spiegel received the Material Engineering degree from Ecole supérieure d'Ingénieurs de Luminy (ESIL) in 2008.

He is with Ion Beam Services, Peynier, France, as an Application Engineer.

Frank Torregrosa received the Ph.D. degree in material science from Ecole nationale supérieure d'Arts et Métiers (ENSAM).

He is a Research and Development Manager with Ion Beam Services, Peynier, France.

Dimitris Tsoukalas received the Diploma degree in electrical and mechanical engineering from the National Technical University of Athens (NTUA), Athens, Greece, in 1979, the Ph.D. degree in electronics and the Habilitation degree from the National Polytechnic Institute of Grenoble (INPG), Grenoble, France, in 1983 and 1994, respectively.

He joined NTUA in 2002, where he is a Professor.